Interannual Westward-Propagating Baroclinic Long-Wave Activity on Line P in the Eastern Midlatitude North Pacific

WARREN B. WHITE

Scripps Institution of Oceanography, University of California, San Diego, La Jolla, CA 92037

SUSUMU TABATA

Institute of Ocean Sciences, Sidney, B.C., Canada, V8L 4B2

(Manuscript received 12 June 1986, in final form 24 September 1986)

ABSTRACT

For the period 1959–81, quasi-zonal hydrographic sections have been made between the southern coast of Vancouver Island (49°N, 126°W) and Ocean Station P (50°N, 145°W) approximately every two months. Along this section (called Line P) hydrographic-STD stations were repeated at nearly the same locations, approximately 2° of longitude apart and at closer intervals near the coast. As such, 13 stations in all were made nearly every two months over the 23-year period. Thus, the Line P dataset has particular value in verifying the existence of interannual baroclinic long waves near 50°N. In previous studies, White, Kang and Magaard, and White and Saur, had found evidence of annual and interannual baroclinic long-wave activity in the eastern midlatitude North Pacific over the range 20°–40°N, but earlier attempts could not discover these westward-traveling waves along Line P. In this study, both spectral analysis and complex empirical orthogonal function analysis are used to do just that. Concentrating upon the depth of the $\sigma_t = 26.8$ density surface, which lay just below the main halocline but within the main pycnocline, the time–longitude matrix of interannual anomalies about the long-term mean annual cycle display westward propagation of much longer period (2–5 years), with speeds similar to baroclinic Rossby waves, over the entire length of the section. The zonal wavenumber/frequency spectrum of this dataset finds the maximum spectral energy density overlying the linear Rossby wave dispersion curve. The first two complex EOFs both show westward propagation, one with larger period/wavelength than the other, both together explaining 46% of the total variance of the 23-year record. Recombining the time–longitude matrix from only these first two complex EOFs shows that the interannual baroclinic long waves tend to be associated with ENSO events that have now been found to occur in both the ocean and the atmosphere throughout the Pacific basin every 2–5 years.

1. Introduction

Early efforts to detect interannual baroclinic long-wave activity in the pycnocline of the eastern midlatitude North Pacific used repeated XBT data taken for the 14-year period (1966–79) along the great circle route from San Francisco near 38°N to Honolulu near 24°N (White and Saur, 1983). Baroclinic long waves of periods of 2–5 years were shown to propagate westward from the coast of North America out along the first third of this section at linear baroclinic Rossby wave speeds, but as the section turned toward the southwest, the waves (refracting toward the northwest) crossed the section normal to it. As such, the presence of baroclinic long waves along this latter portion of the section could be inferred only indirectly by the subsequent success of amplitude and phase of the model/data intercomparison (i.e., a model of Ekman pumping alone could account neither for the amplitude nor the phase). Yet, in two other studies (White, 1982, 1985), interannual baroclinic (Rossby) waves were shown to propagate directly westward from the coast of North America in the main thermocline (i.e., near 125°W) out to 165°W along a constant latitude section at 40°N for the 4-year period 1976–80, made possible by the XBTs deployed by the TRANSPAC Volunteer Observing Ship (VOS) program (White and Bernstein, 1979).

To date, the discovery and subsequent investigation of the interannual baroclinic long-wave activity in the eastern North Pacific has been primarily restricted to regions where the subsurface thermal structure has been measured repeatedly over many years (White and Bernstein, 1979). A most obvious dataset with which to extend this investigation is that consisting of the repeated hydrographic sections (i.e., observations made by STD recorders and Nansen–Niskin bottle casts) made along Line P, extending from the southern coast of Vancouver Island at 49°N, 126°W to Ocean Station P at 50°N, 145°W (Fig. 1). Earlier, Willmott and Mysak (1980) had studied two-dimensional interannual Rossby waves in connection with semipermanent eddies located off the coast of British Columbia and Alaska, but they did not utilize the Line P dataset. The

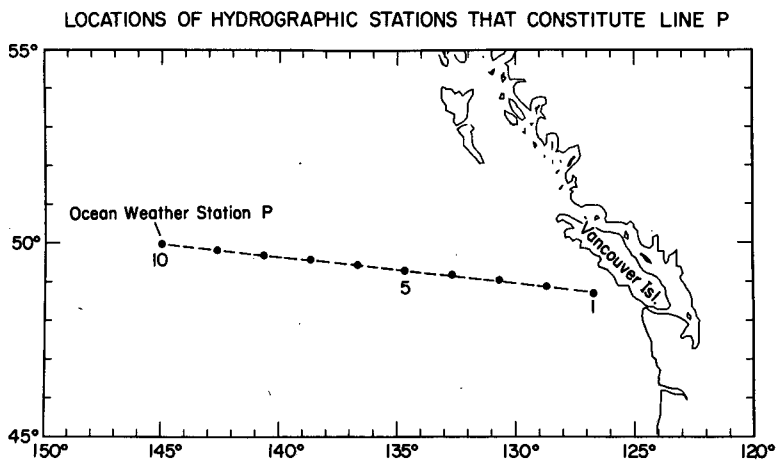

FIG. 1. Geographic location of Line P, extending from the southern coast of Vancouver Island to Ocean Station P.

hydrographic section along Line P was occupied approximately every two months during 23 years from 1959–81. Only those stations that were repeated over most of the section at approximately 2° longitude intervals were used in this study; others near the coast over the continental shelf were deleted from consideration.

Therefore, in this study the hydrographic data from the Line P section is examined for baroclinic, long-wave activity. The depth of the density surface where $\sigma_t = 26.8$ is chosen as the representative isopycnal surface of our study. In this region, the interannual variability of the surfaces of $\sigma_t = 26.2$ through 26.7 were in phase (Tabata et al., 1986), and therefore, any one of these surfaces could have been used. This density surface is in the main pycnocline over the entire length of Line P and allows internal geostrophic waves to be detected. Because these data were not taken exactly two months apart, they were first interpolated onto a regular bimonthly time grid. Next, the long-term annual and bimonthly means were computed, leading to the computation of anomalies about the mean annual cycle. Because gaps remained in the anomaly data, these were filled using maximum entropy methodology. The subsequent dataset of anomalies was then used to form zonal wavenumber/frequency spectra and complex empirical orthogonal functions, both of which are consistent with the presence of interannual linear baroclinic Rossby waves near 50°N.

2. Data and methods

The locations of the 10 repeated hydrographic stations taken along Line P that are used in this study are displayed in Fig. 1, with stations located approximately 2° of longitude apart from 49°N, 126.7°W off the southern coast of Vancouver Island to 50°N, 145°W, the location of Ocean Station P. Two repeated stations in the original Line P series have been deleted, one near the coast because it was on the continental shelf and the other because it did not conform to the 2° longitude spacing. The resulting 10 stations in Fig. 1 were occupied approximately every two months for 23 years extending from 1959 to 1981, as indicated in Fig. 2. In this latter figure, the 23-year time record can be seen to have had gaps of up to 6-months duration (in 1959–61, 1964–65, 1966–67, 1968, 1970–71, 1974–75, 1975–76 and 1979–80), but much of the rest of the time record is relatively complete. Generally, the space record is complete as well; i.e., when a section existed in time, usually all of the stations of the Line P were occupied. When this was not true, stations were missing due mainly to inclement weather. In a few cases, stations were removed by an editing procedure that designated them as being of poor quality.

As can be ascertained from Fig. 2, the station locations were not occupied exactly at two-month intervals. For subsequent analysis it is necessary to have data at uniform time spacing. Therefore, a cubic spline interpolation routine was applied to the time record at each station location, placing these values onto a regular two-month time grid, centered on the bimonth. The cubic spline procedure has an advantage over other interpolation procedures because it does the least amount of smoothing of the overall record. Data gaps of 1–2 bimonths in duration were filled with this interpolation procedure. Gaps of greater than 2 bimonths were filled using maximum entropy methodology.

The maximum entropy method (MEM) of spectral estimation was developed by Burg (1967, 1968) to increase spectral resolution when the lengths of the available data records were shorter than required to conduct fast-Fourier transforms. Prior to the development of MEM, the usual method of increasing resolution had been to append a sequence of zeroes to the data sequence prior to transforming. The maximum entropy

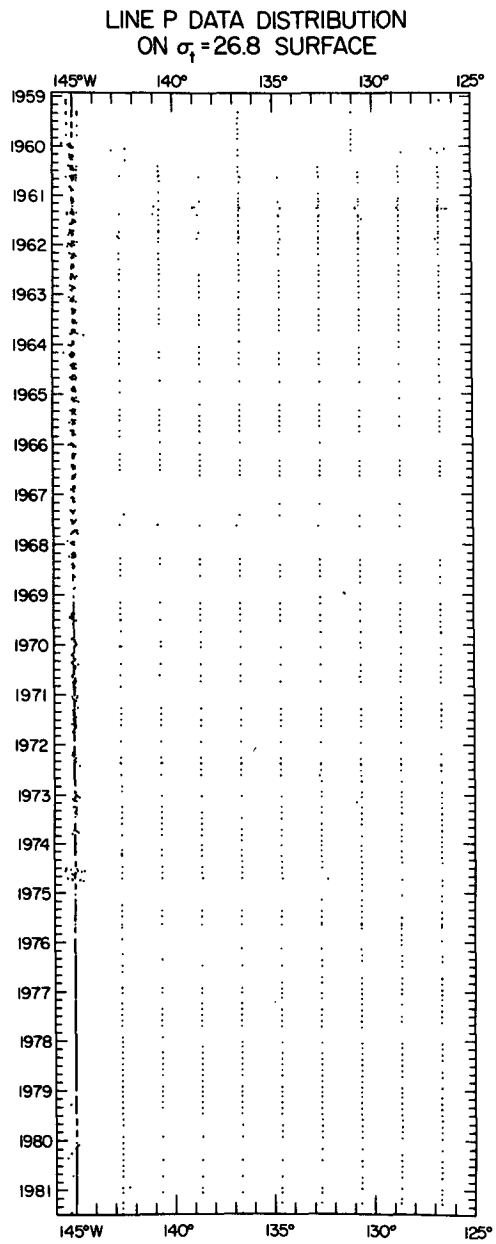

FIG. 2. The time–longitude locations of hydrographic stations that have constituted the Line P section from 1959–81. These stations represent those that have been edited from a larger file.

method extrapolates the data record beyond its given length using information of the correlation structure of the available data series. This method predicts the ith value of the sequence by

$$Z_i = \sum_{k=1}^{N} a_k Z_{(i-k)}, \quad i \geq N+1, \tag{2.1}$$

where the predicted value Z_i is calculated by summing the products of the prediction coefficients, a_k, with the past N values of the data, $Z_{(i-k)}$. The coefficients, a_k, are determined by minimization, in a least-squares sense, of the quantity E^2, where

$$E^2 = \sum_{i=N+1}^{M} \{Z_i - \sum_{k=1}^{N} a_k Z_{(i-k)}\}^2, \tag{2.2}$$

where M is the number of points in the data gap. The minimization of (2.2) yields a set of linear equations that can be solved for a_k most quickly using the recursive method outlined by Andersen (1974). Therefore, the extrapolation beyond the length of the data record is equivalent to least-squares fitting of an Nth order model to the data (Van Den Bos, 1971). Restrictions placed on this extrapolation procedure are that the number of data points before the gap (i.e., N) must be at least twice the gap length, (i.e., M), and preferably much greater.

3. Mean, rms differences, and annual cycle of the depth of the σ_t = 26.8 density surface

As explained in the Introduction, the parameter chosen to detect interannual baroclinic long-wave activity is the depth of the σ_t = 26.8 density surface. The annual long-term mean depth of that density surface and the root-mean-square (rms) differences is given in Fig. 3. The mean depth of the 26.8 density surface is seen to be 325 m at 127°W off the southern coast of Vancouver Island, decreasing to the west in a nearly linear fashion to 200 m at 145°W, the location of Ocean Station P. The rms differences of the individual bimonthly values of σ_t depth, about the annual long-term mean depth for the 23-year period, are largest next to the coast of Vancouver Island (i.e., ±39 m), decreasing to the west to a minimum value (i.e., ±20 m) at 141°W.

As will be demonstrated in a later section, much of the rms variability appears to have been associated with

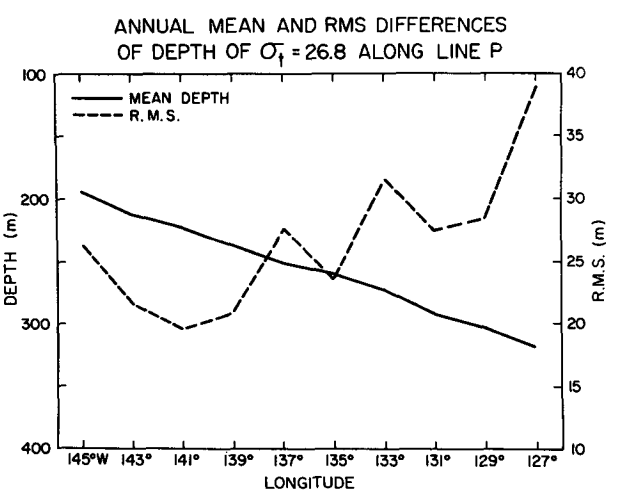

FIG. 3. Long-term annual mean and rms differences about that mean of the depth of the σ_t = 26.8 density surface along Line P.

baroclinic long-wave activity originating near the coast of Vancouver Island. The observation that the mean depth of the σ_t = 26.8 surface decreases toward the west indicates that Line P intersects the mean northward shear of the Alaska Current. Therefore, these waves are directed approximately normal to this mean shear flow. According to Killworth (1979), this mean shear flow will have an effect upon the westward propagation of linear baroclinic Rossby waves by decreasing the speed of the waves through the decrease in the internal radius of deformation (i.e., $[|g'H/f^2]^{1/2}$, where H is the depth of main pycnocline and g' is reduced gravity in a two-layer ocean, with the lower layer at rest). Therefore, it may be expected that linear baroclinic Rossby waves will have significantly reduced westward speed (i.e., $C_{px} = -\beta/[k^2 + l^2 + (f^2/g'H)]$) as they propagate to the west (i.e., as H decreases). Moreover, they will be refracted by this effect, as well as by the effect of β dispersion (Schopf, et al., 1981). Furthermore, the propagation of energy (i.e., group velocity) will also change due to this effect. It is possible that with these changes in the dispersion relationship along Line P nonlinear effects may become important, affecting the amplitude of these waves. In subsequent discussion, the effects of both the mean baroclinic flow and possible, but unknown, barotropic flow will be neglected when relating the linear Rossby wave analysis to these observed interannual baroclinic long waves. For the most part, the linear theory explains most of what is seen, but of course, it cannot explain everything. This we leave for a future modeling effort.

The observation that the rms differences in the depth of the σ_t = 26.8 surface were largest next to the coast, decreasing toward the west, is consistent with the earlier observation of rms differences of subsurface temperature of 40°N (White, 1985). As shown in this earlier study, larger rms differences next to the coast were related to larger rms differences in wind stress curl near the coast, generating baroclinic long (Rossby) waves at the coast through the mechanism of Ekman pumping. White and Saur (1983) determined that rms differences in wind stress curl were even larger next to the coast of Vancouver Island at 50°N than next to the California coast at 40°N. Therefore, although no causal connection is made in this study between baroclinic long (Rossby) wave activity and the wind stress curl at 50°N, the intensification of both adjacent to the coast is consistent with the earlier study (i.e., White and Saur, 1983) and suggests a wind-driven origin for the pycnocline variability observed at the coast. The quantitative demonstration of this is left for later study.

The annual cycle of the depth of the σ_t = 26.8 density surface about the long-term annual mean, based upon long-term bimonthly values computed over the 23-year period, is given in Fig. 4. It shows westward propagation from the coast out to approximately 133°W, at a zonal speed of approximately 2 cm s^{-1}. This speed is about twice the celerity of baroclinic Rossby waves (i.e., ~1.1 cm s^{-1}) at this latitude (Mysak, 1983); moreover, it is very near the critical latitude of linear baroclinic Rossby waves (White, 1982; Mysak, 1983). Therefore, this wave propagation may not be a manifestation of annual Rossby waves, but simply forced by the annual cycle of the wind. To determine whether this is true will require the operation of a wind-driven model of baroclinic Rossby wave activity, again beyond the scope of the present investigation. West of approximately 133°W, the westward propagation in the annual cycle in Fig. 4 disappears.

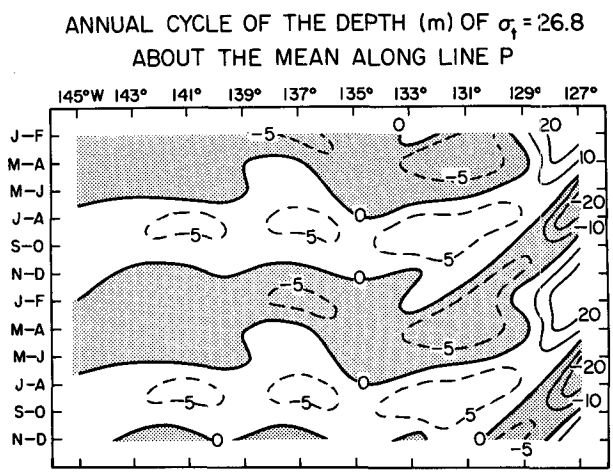

FIG. 4. Annual cycle of the long-term bimonthly mean depth of σ_t = 26.8 density surface about the long-term annual mean along line P. Two cycles are shown in time. Positive values indicate that the σ_t = 26.8 surface is deeper than the long-term annual mean; negative values indicate shallower depths.

4. Anomalous depth of the σ_t = 26.8 density structure

The anomalous depth of the σ_t = 26.8 density surface along Line P is computed by subtracting the bimonthly long-term mean values from the individual values each bimonth. The resulting time–longitude matrix is displayed on the left-hand panel of Fig. 5 for the period January 1963 to June 1981. Data prior to 1963 were deleted because of their relative paucity. This time–longitude matrix is contoured where data exist; gaps in the data occur where the contours are discontinued.

For subsequent analysis, it is desirable to fill these data gaps; this is accomplished using the maximum entropy method described in section 2. This procedure essentially extrapolates into the gaps using the data and its correlation structure occurring before the gap. This filled data matrix is then normalized by the rms in both time and space. The normalization procedure suppresses spatial and temporal changes (i.e., nonstationarities) in the variance of the filled data matrix. Lastly, the time–longitude data matrix is detrended in time. The resulting processed anomalies (i.e., filled, normalized and detrended) are displayed in the right-hand panel of Fig. 5. They show evidence of westward

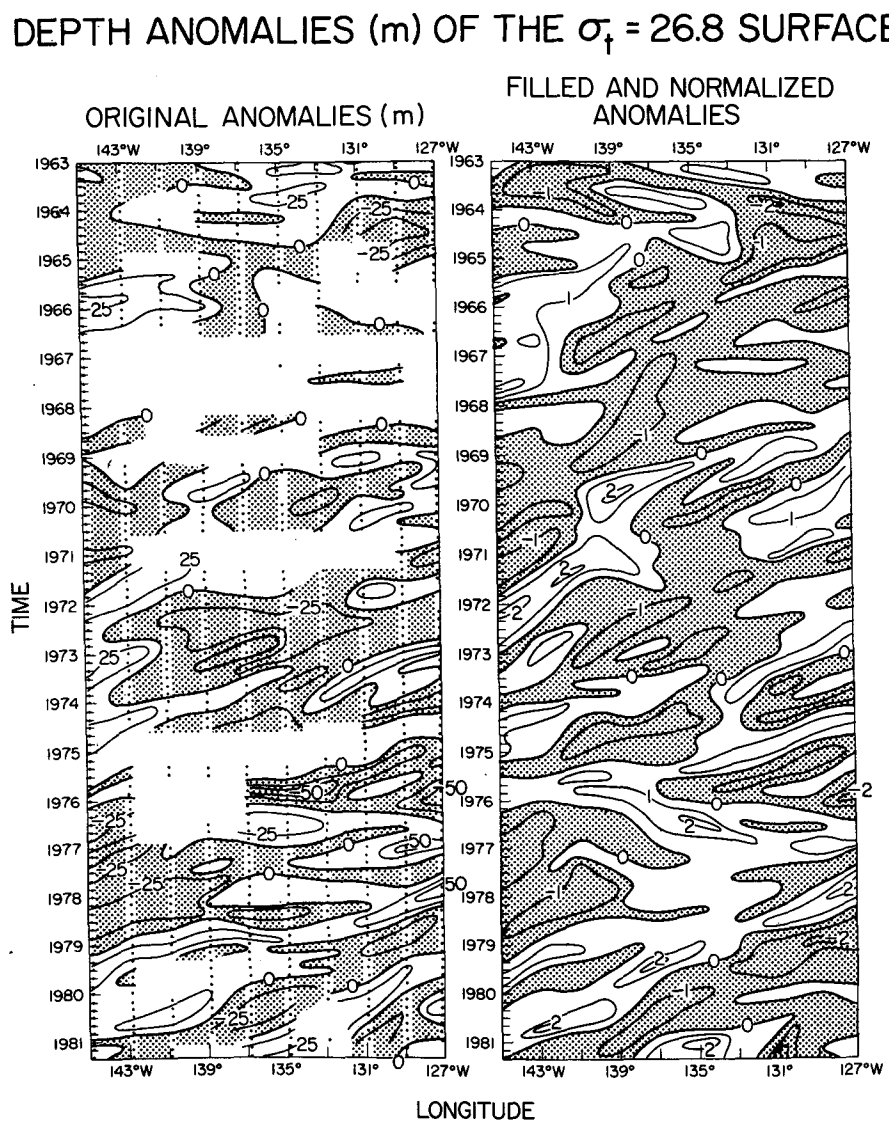

FIG. 5. Time–longitude matrices of anomalous depth of the σ_t = 26.8 density surface along Line P, extending in time from 1963 to 1981. On the left are the raw anomalies based upon individual bimonthly means; on the right are the processed anomalies with gaps filled, normalized and detrended (see text for further details). Positive values indicate that the σ_t = 26.8 surface is deeper than the long-term bimonthly mean; negative values indicate shallower depths.

propagation, with contours extending westward with increasing time. The zero contours are approximately parallel to those in the unfilled time–longitude matrix (left panel, Fig. 5), with differences attributed to the detrending procedure. Some evidence of eastward propagation can also be seen (e.g., 1963, 1977), but it occurs rarely. The westward propagation that can be seen appears to have a dominant speed (i.e., approximately 1 cm s^{-1}), but some variability (as much as 100%) occurs about that.

Westward propagation in the time–longitude matrix of processed anomalies is confirmed, and a dominant speed determined, from the frequency/zonal wavenumber spectrum (upper panel, Fig. 6). This frequency/zonal wavenumber spectrum is computed using the standard Blackman and Tukey (1958) method with a Parzen window with 8 lags (in both dimensions). This yielded 22 degrees of freedom for the spectrum. The contour interval equals the 90% confidence interval for this number of degrees of freedom. Thus, the peak at a period of 3–5 years and a wavelength of 10°–20° longitude is statistically significant. No filters other than the Parzen window, normalization and detrending in time were used.

This spectrum shows the maximum spectral energy density at a period of 3–5 years lying on the linear

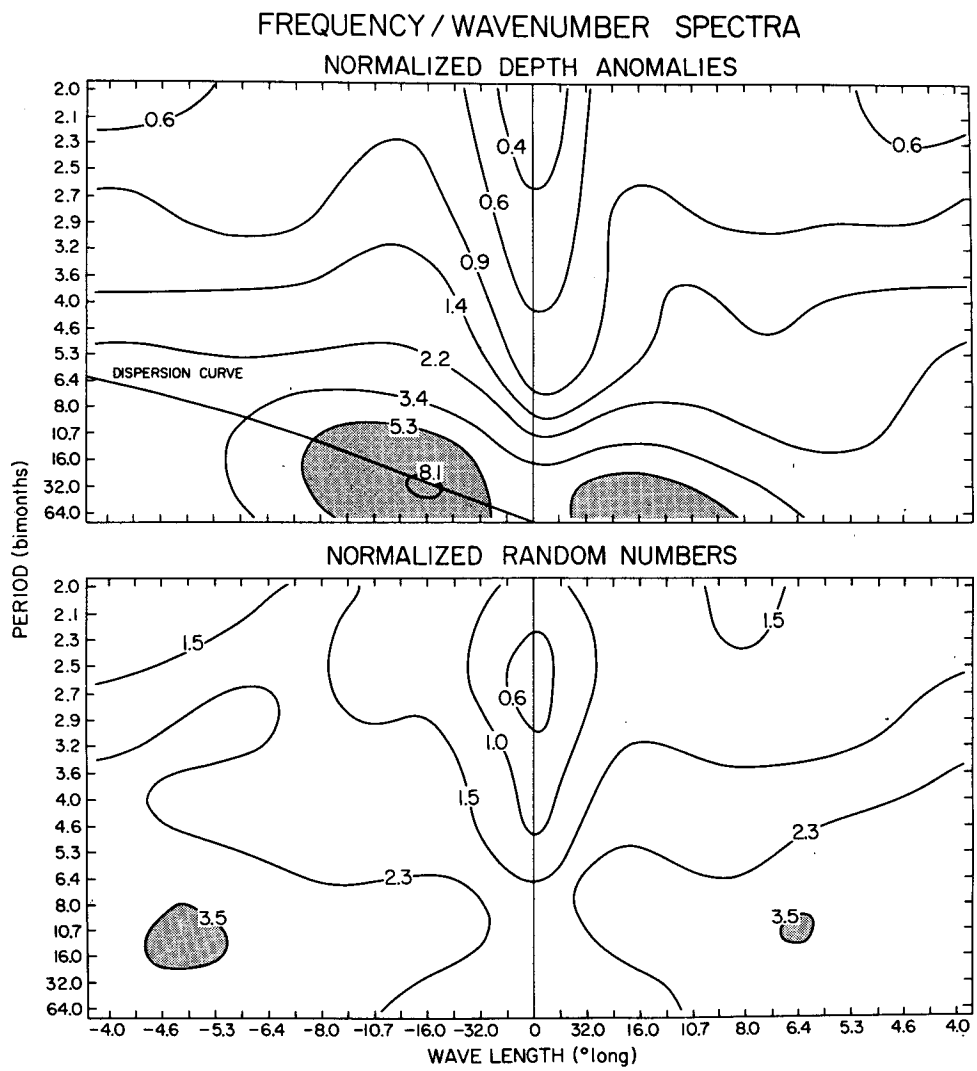

FIG. 6. Frequency/zonal wavenumber spectrum of processed anomalies of the depth of the σ_t = 26.8 density surface along Line P. The contour intervals are the 90% confidence intervals. The linear Rossby wave dispersion curve is also displayed (see text for further details). Wavelength is in degrees of longitude; period is in bimonths (i.e., 2-month lengths).

baroclinic Rossby wave dispersion curve, which extends toward negative wavenumber with positive frequency; i.e.,

$$\omega = \frac{-\beta k}{k^2 + l^2 + \alpha^2}, \tag{4.1}$$

where ω is the frequency, k the zonal wavenumber, l the meridional wavenumber, α^{-1} the internal radius of deformation, and β the meridional derivative of the Coriolis parameter f. Over most of the wavenumber domain displayed, the zonal wavenumber k is very small compared to the inverse internal radius of deformation (i.e., α^{-1} = 30 km); therefore, (4.1) reduces to the long-wave (nondispersive) relation where ω and k are linearly related. As such, the zonal phase speed is

$$C_{px} = \frac{\omega}{k} = \frac{-\beta}{\alpha^2} = \frac{-\beta g' H}{f^2}, \tag{4.2}$$

where f is the Coriolis parameter, g' reduced gravity, and H the depth of the upper layer (i.e., pycnocline) of a two-layer ocean with the lower layer at rest. In Fig. 6, the zonal wave speed (i.e., C_{px}) is calculated to be 1.1 cm s^{-1}, where H = 250 m and g' = 3 cm s^{-2}; this value of the speed is similar to that produced by Mysak (1983). As discussed earlier, this dispersion relation derives from a linear model that ignores the effects of barotropic and baroclinic background flows, bottom bathymetry effects, etc.

This frequency/zonal wavenumber spectrum in the upper panel of Fig. 6 is compared with the corresponding spectrum of random data, displayed in the lower

panel of Fig. 6. Random data was used to replace real data at the location of the hydrographic stations in Fig. 2. Then, these random data were treated in the same manner as the real data (i.e., a cubic spline was used to construct the bimonthly grid); the maximum entropy method was used to fill the gaps greater than 2 bimonths; the data were normalized and detrended in time; and the frequency/wavenumber spectrum was computed with the Blackman and Tukey (1958) method using a Parzen window with 8 lags. The resulting zonal wavenumber/frequency spectrum of these random data does not show the maximum values along the Rossby wave dispersion curve. For periods less than 1 year (i.e., 6 bimonths), both spectra are similar and nearly symmetric for $\pm k$ (i.e., zonal wavenumber), indicating that the real data anomalies tend to randomness at these shorter periods.

5. Complex empirical orthogonal function analysis

The time–longitude matrix of anomalous depth of $\sigma_t = 26.8$ density surface is seemingly composed of interannual baroclinic long-wave activity of the type observed by White (1982) at 40°N. Upon closer inspection, there is the suggestion in these data and in earlier studies of temperature fluctuations at Ocean Station P and N (e.g., White and Walker, 1974) that the large-scale variability is related to ENSO (El Niño/Southern Oscillation) events occurring most prominently in the equatorial and tropical Pacific ocean–atmosphere environment. In order to investigate this possibility more thoroughly, the time–longitude matrix of the processed anomalous depth of the $\sigma_t = 26.8$ density surface is operated upon by complex empirical orthogonal function analysis. This analysis has the capability of separating the dominant time–space variability (i.e., defined here as the signal) from the less dominant and random variability (i.e., defined here as the ambient noise).

Complex EOF analysis (also known as complex principal component analysis) has the ability to detect both standing and traveling wave phenomena in the 19-year (1963–83) time–longitude matrix of processed depth anomalies of the $\sigma_t = 26.8$ density surface displayed in Fig. 5. Compared to the more conventional real EOF analysis (Lorenz, 1956), the complex EOF has an additional step. Given an anomalous dataset denoted $d_j(t)$, where j denotes spatial position and t is time, this additional step is the generation of a complex anomalous data field $D_j(t)$, whose real part is the original data field $[d_j(t)]$ and whose imaginary part is the data field $[\hat{d}_j(t)]$. This imaginary part of the complex data field has the same spectrum as the real data field but with the phase at every frequency shifted 90° from that of the original data field. This is accomplished by applying a Hilbert transform to the original data field. The 90° phase shift of each Fourier component is equivalent to providing optimal lag information on that component, allowing traveling wave activity in the real field to be detected.

Once the complex data field is known, the same procedure for determining the eigenvectors and principal components of the real dataset is used, except that the procedure is applied to both real and imaginary data fields. Then, the results of the complex EOF analysis are represented in terms of the amplitude and phase of the complex eigenvectors (i.e., representing spatial variability) and the complex principal components (i.e., representing time variability) of the complex data field. A rigorous discussion of these procedures is given in both Horel (1984) and White et al. (1987).

The first two complex EOFs of the anomalous depth of the $\sigma_t = 26.8$ density surface are displayed in Fig. 7, together accounting for 46% of the total interannual variance contained in the time–longitude matrix in Fig. 5. According to significance tests developed by Barnett (1977) and Preisendorfer and Barnett (1977), the two EOFs shown in Fig. 7 are determined not to have been derived from random data. The next higher order EOFs (i.e., 3–5) did not pass this test. Yet, it is important to note that these higher order EOFs also demonstrated a strong tendency for westward propagation of the anomalies, explaining 15%, 13% and 10% of the variance, respectively (not shown). However, according to the statistical analyses conducted by North et al. (1982), individual EOFs of similar variance (i.e., as in the case of complex EOFs 1 and 2 in Fig. 7) are interpreted as dependent components of a set of EOFs that together describe the same statistical process. In this case, the first two complex EOFs, which explain 25% and 21% of the total variance, respectively, are therefore not statistically independent. Although they are orthogonal to each other (i.e., linearly independent), they are a part of very similar statistical processes. This is perhaps obvious, since both the wavenumber $(\partial\phi/\partial x)$ and frequency $(\partial\phi/\partial t)$ of these two EOFs are relatively monotonic and of similar sign.

The first two complex EOFs have spatial patterns that are very similar. The amplitude tends to increase with distance away from the southern coast of Vancouver Island; the phase increases montonically to the west with distance, indicating westward direction of the zonal wavenumber (i.e., $k = \partial\phi/\partial x$). The corresponding wavelength scale can be easily seen to be 18° of longitude for the first complex EOF and approximately half that (10° of longitude) for the second EOF. The shorter wave propagates to 140°W, but not west of there, whereas the longer wave propagates westward over the entire longitudinal extent of Line P (i.e., out to at least 145°W).

The two time sequences of amplitude are orthogonal to one another, displaying variability of little significance. However, the time sequences of phase show monotonic time phase development, with the first complex EOF displaying generally lower frequency (i.e., $\partial\phi/\partial t$) scale and more interannual variability in

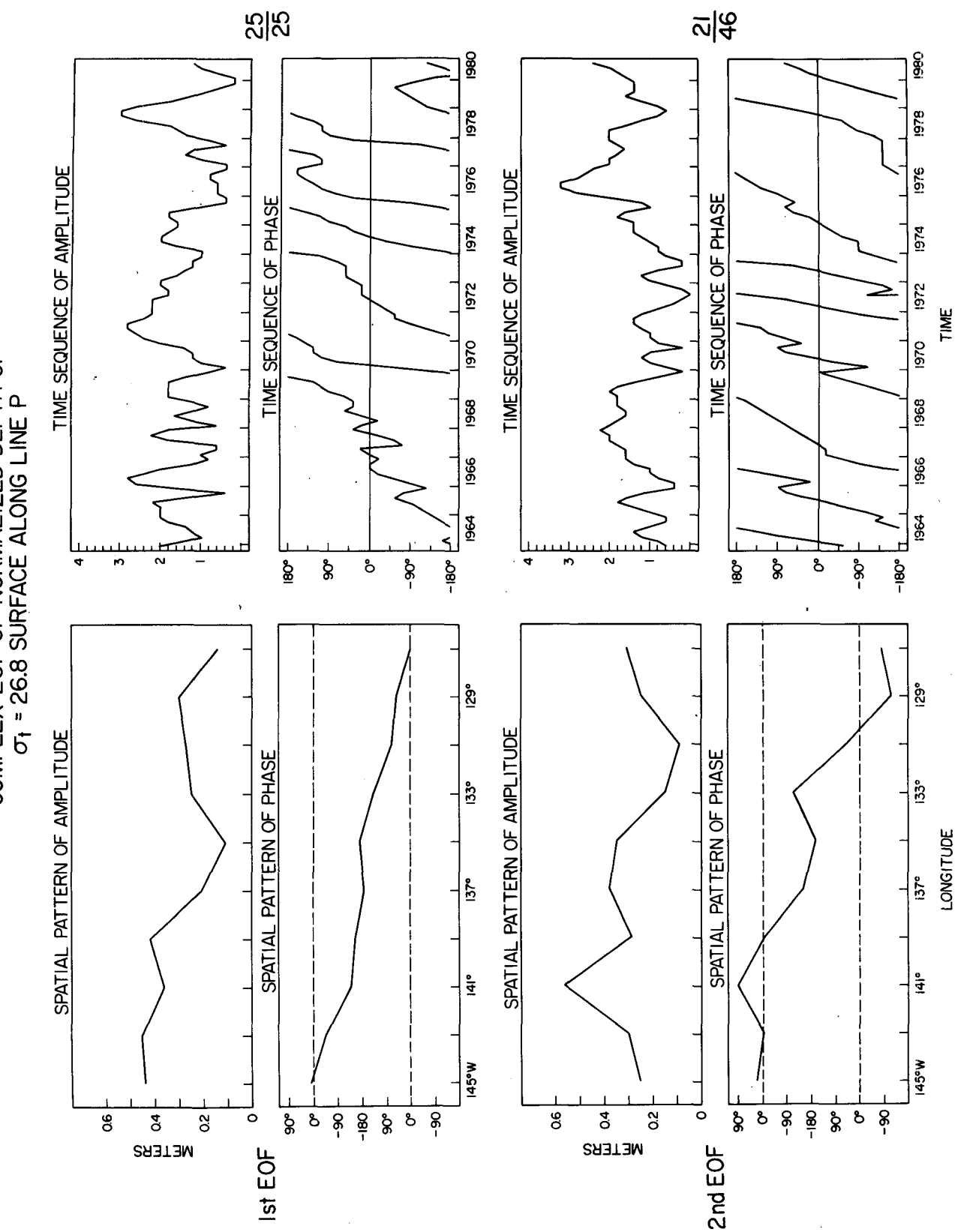

FIG. 7. Complex EOF analysis of the processed anomalies of the depth of the σ_t = 26.8 density surface. The first two functions are displayed, each with similar variance explained (i.e., 25% and 21%, respectively). The spatial patterns of amplitude and phase are on the left, with the time sequences of amplitude and phase on the right. Spatial phase increasing to the west, associated with temporal phase increasing with time indicates [illegible]

frequency than the second complex EOF. The second complex EOF can be seen to have a period scale of approximately 1–3 years (i.e., the time it takes for the phase to extend over 360°), while the first EOF has period scales ranging from 2 to 5 years. Time phase development occurring when the amplitude is very low can be neglected from consideration.

Therefore, the first complex EOF has a zonal wavelength scale of approximately 18° longitude, associated with period scales of 2–5 years, while the second complex EOF has a zonal wavelength scale of approximately 8° longitude associated with period scales of 1–3 years. These scales broadly straddle the linear Rossby wave dispersion curve given in Fig. 6, without verifying the linear theory; such verification can occur only when a model can be constructed that will simulate the amplitude and phase as a function of space–time. These results are also consistent with the frequency/zonal wavenumber spectrum, which has greater spectral energy density at the longer wavelengths/periods.

6. Discussion and conclusion

The complex EOF analysis acts as a filter separating low frequency variability from higher frequency variability. The low frequency variability tends to be more deterministic, while the higher frequency variability is more stochastic, as observed in wavenumber/frequency spectra in Fig. 6. It is possible to see this by reconstructing the time–longitude matrix in Fig. 8, with much of the higher frequency variability removed, by using just the first 2 complex EOFs in Fig. 7. This process yields only the variance contained in these first 2 complex EOFs, which has been shown in the previous section to be dominated by westward-traveling baroclinic long-wave activity of wavelengths 10°–20° longitude and periods of 1–5 years. The reconstructed time–longitude matrix is given in Fig. 8 and displays this wave propagation clearly. Yet, the obvious change in speed with time displayed in this figure suggests that the background baroclinic and barotropic conditions are nonstationary.

This time–longitude matrix shows waves of period scale ranging from 1 to 5 years emanating from the southern coast of Vancouver Island, propagating westward, and gaining amplitude in the direction of propagation out to Ocean Station P. This is very similar to that observed at 40°N by White (1982), with the increasing amplitude in the direction of propagation consistent with the theory exploited by White (1985) on the resonant driving of the baroclinic long (Rossby) waves by the overlying wind stress curl field. It remains to be seen whether such a resonant wind-driving model can explain the actual phase of these waves (as White, 1985, was able to do at 40°N).

The earlier work of Horel and Wallace (1981) linked the pressure patterns in the Gulf of Alaska to ENSO events in the equatorial and tropical Pacific. Therefore, it may be expected that a phase relationship exists between anomalies along Line P and ENSO events that exist in the tropical Pacific, provided these anomalies are either directly or indirectly wind driven. In Fig. 9 is the detrended time sequence of the anomalous sea level at Callao (12°S) along the coast of Peru, observed by White et al. (1987) as indicative of ENSO events in the eastern tropical Pacific. Also shown are the time sequences of depth anomalies of the $\sigma_t = 26.8$ isopycnal surface taken from Fig. 8 at three locations along Line P. The shaded bands indicate the ENSO years, with sea level (and pycnocline depth) tending to peak at Callao sometime during these years. Also shown at the bottom of the figure is the correlation matrix between

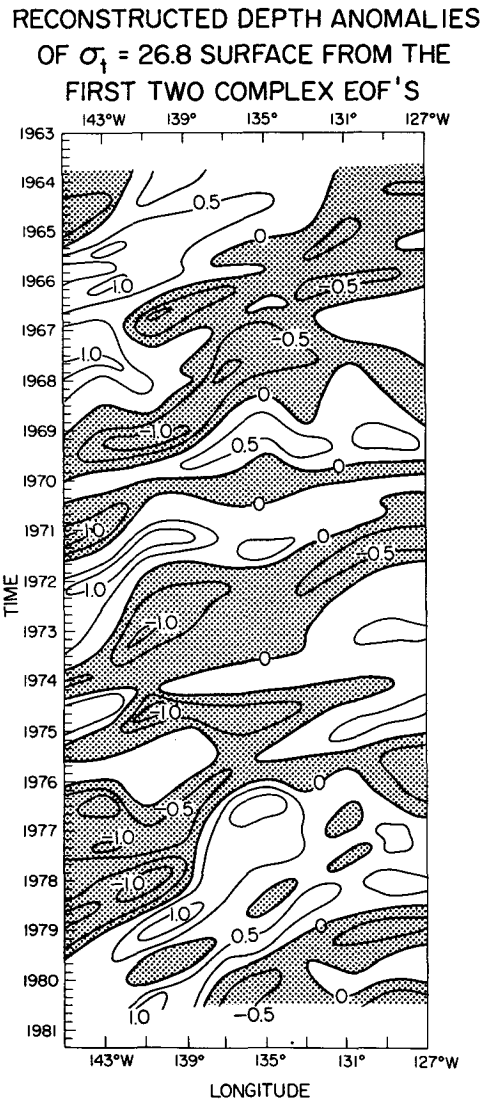

FIG. 8. Reconstructed time–longitude matrix of the normalized anomalous depth of the $\sigma_t = 26.8$ density surface, based upon the first two complex EOFs displayed in Fig. 7. This matrix contains 46% of the variance displayed for the time–longitude matrix on the right hand side of Fig. 5.

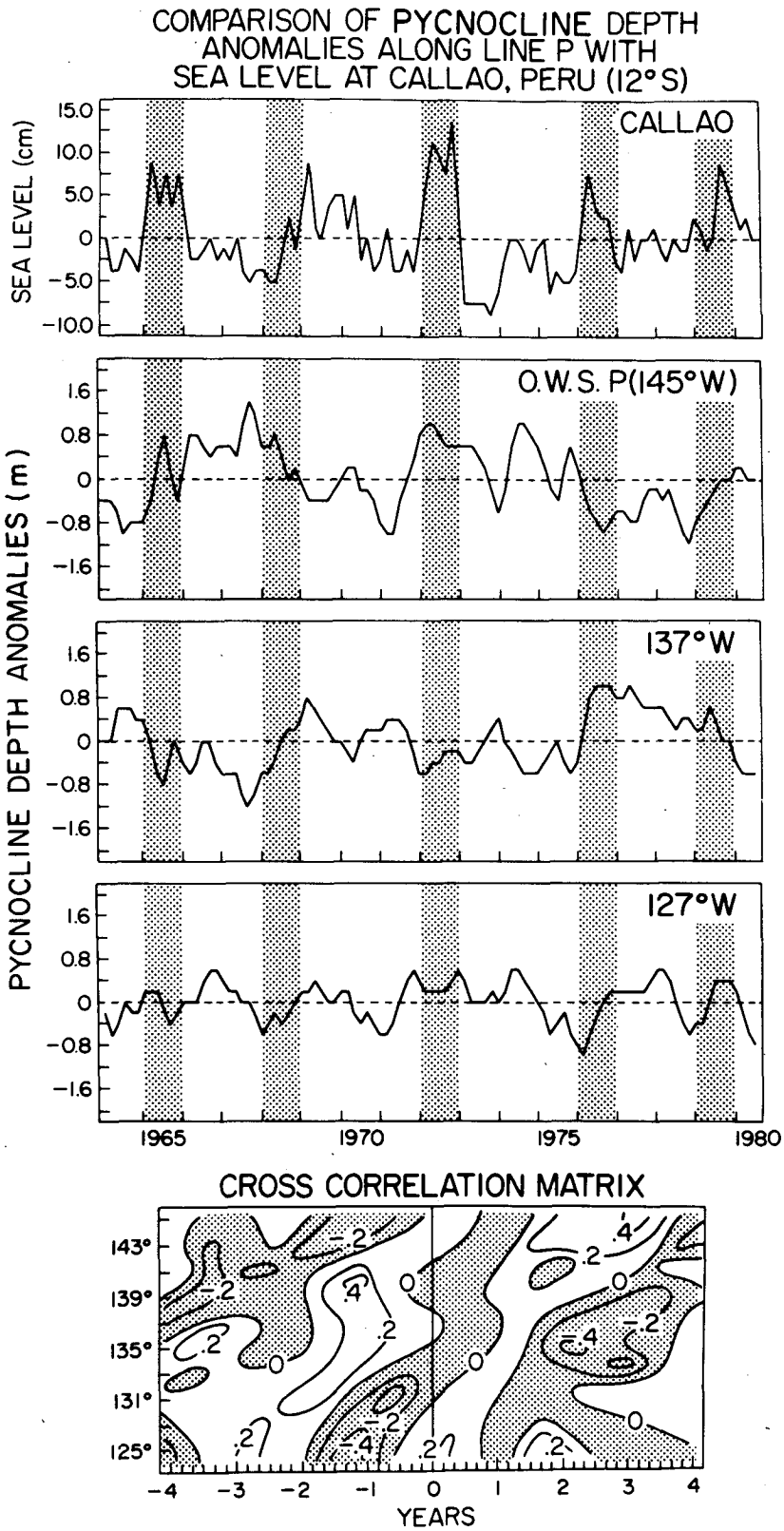

FIG. 9. (Top panel) Time sequence of detrended sea level anomalies at Callao, Peru (12°S), from 1963 to 1981, together with time sequences of depth anomalies of the $\sigma_t = 26.8$ isopycnal surface at three locations along Line P taken from Fig. 8. The shaded bands represent years

the Callao time sequence and all of the time sequences along Line P from Fig. 8.

This correlation matrix at the bottom of Fig. 9 has the time sequence at Callao correlating positively with the anomalous depth of the $\sigma_t = 26.8$ isopycnal surface near the southern coast of Vancouver Island at zero lag. At approximately 18 degrees of freedom [determined by dividing the record length by the decorrelation scale of the record (Bendat and Piersol, 1971)], cross correlations equal to 0.4 are significant at the 90% confidence level. Therefore, during ENSO events, the pycnocline depth at Callao and the pycnocline depth at the southern coast of Vancouver Island were both deeper than normal, but at a correlation that is below this significance level. However, this positive correlation is maintained consistently along Line P with time from the southern coast of Vancouver Island out to Ocean Station P, being correlated positively there significantly three years later. This significant positive correlation at Ocean Station P is larger in general than those correlations along Line P because of the much larger number of data taken there (see Fig. 2). These positive cross correlations, extending westward with time along Line P, are indicative of the influence of baroclinic long-wave activity along Line P and, in fact, have a slope (i.e., 1–2 cm s^{-1}) in lag space approximating the phase speed (i.e., $\sim$1 cm s^{-1}) of the linear baroclinic Rossby waves.

One year prior to the ENSO event, the depth anomaly of the $\sigma_t = 26.8$ isopycnal surface is significantly negatively correlated with the pycnocline depth anomaly at Callao. This means that one year in advance of ENSO events the pycnocline depth of the southern coast of Vancouver Island was shallower than normal. This is very interesting because it suggests that there may be phenomena in the atmosphere at midlatitude that act as a precursor to ENSO events in the eastern tropical Pacific. In fact, this is consistent with the observation by Namias (1976) that weak winter pressure patterns in the northeast Pacific often precede major tropical El Niño events by one year. Similar results were more recently observed by Emery and Hamilton (1985).

Therefore, the development of the ENSO event in the Pacific extends to midlatitude not only in the atmosphere, as Horel and Wallace (1981) and others have found, but in the ocean as well, and, at least locally, the development is associated with baroclinic long waves that are probably driven by the anomalous wind stress that occurs in association with the meridional teleconnections associated in the atmosphere with ENSO events.

Acknowledgments. Much appreciation is given to Lawrence Mysak and Robert Haney for their contributions in improving the discussion contained within this manuscript. Both Arthur Walker at SIO and David Ramsden at IOS, as programmers, were instrumental in conducting the statistical analyses presented in this manuscript. This research was conducted both at Scripps Institution of Oceanography, University of California at San Diego, and the Institute of Ocean Sciences in Sidney, British Columbia. At SIO, this research was sponsored by the Office of Naval Research through Contract N-00014-75-C-0152 through the Ocean Research Division.

REFERENCES

Andersen, M., 1974: On the calculation of filter coefficients for maximum entropy analysis. *Geophysics,* **39,** 69–72.

Barnett, T. P., 1977: The principal time and space scales of Pacific trade wind fields. *J. Atmos. Sci.,* **34,** 633–647.

Bendat, J. S., and A. G. Piersol, 1971: *Random Data: Analysis and Measurement Procedures.* Wiley Interscience, 407 pp.

Blackman, R. B., and J. W. Tukey, 1958: *The Measurement of Power Spectra.* Dover, 190 pp.

Burg, J. P., 1967: Maximum entropy spectral analysis. Presented at the 37th Annual International Meeting, Soc. of Explor. Geophys., Oklahoma City.

——, 1968: A new analysis technique for time series data. Presented at Advanced Study Institute on Signal Processing, NATO, Enschede, Netherlands.

Cummins, P. F., L. A. Mysak and K. Hamilton, 1986: Generation of annual Rossby waves in the North Pacific by the wind stress curl. *J. Phys. Oceanogr.,* **16,** 1179–1189.

Emery, W., and D. Hamilton, 1985: Atmospheric forcing of interannual variability in the northeast Pacific Ocean: Connections with El Niño. *J. Geophys. Res.,* **90,** 857–868.

Horel, J. D., 1984: Complex principal component analysis: Theory and examples. *Climate Appl. Meteor.,* **23,** 1660–1673.

——, and J. M. Wallace, 1981: Planetary-scale atmospheric phenomena associated with the Southern Oscillation. *Mon. Wea. Rev.,* **109,** 813–829.

Kang, Y. Q., and L. Magaard, 1980: Annual baroclinic Rossby waves in the central North Pacific. *J. Phys. Oceanogr.,* **10,** 1159–1167.

Killworth, P., 1979: On the propagation of stable baroclinic Rossby waves through mean shear flow. *Deep-Sea Res.,* **26A,** 997–1031.

Lorenz, E., 1956: Empirical orthogonal function and statistical weather prediction. Rep. No. 1, Statistical Forecasting Program, Dept. of Meteorology, MIT, 44 pp.

Mysak, L., 1983: Generation of annual Rossby waves in the North Pacific. *J. Phys. Oceanogr.,* **13,** 1909–1923.

Namias, J., 1976: Some statistical and synoptic characteristics associated with El Niño. *J. Phys. Oceanogr.,* **6,** 130–138.

North, G. R., T. L. Bell, R. F. Callahan and F. T. Moeng, 1982: Sampling errors in the estimation of empirical orthogonal functions. *Mon. Wea. Rev.,* **110,** 699–706.

Preisendorfer, R. W., and T. P. Barnett, 1977: Significant tests for empirical orthogonal functions. *Preprints Fifth Conf. on Probability and Statistics in Atmospheric Sciences,* Las Vegas, Amer. Meteor. Soc., 169–172.

in which ENSO events occurred. (Bottom panel) Cross correlation matrix of the time sequence of the detrended sea level anomalies at Callao with the time sequences of depth anomalies of the $\sigma_t = 26.8$ isopycnal surface at each station along Line P (taken from Fig. 8) for the period 1963–81. Negative correlations are shaded; positive correlations are not. Correlations greater than 0.4 are significant at the 90% confidence interval, with approximately 18 degrees of freedom.

Schopf, P. S., D. T. Anderson and R. Smith, 1981: Beta-dispersion of low frequency Rossby waves. *Dyn. Atmos. Oceans,* **5,** 187–214.

Tabata, S., B. Thomas and D. Ramsden, 1986: Annual and interannual variability of steric sea level along Line P in the northeast Pacific Ocean. *J. Phys. Oceanogr.,* **16,** 1378–1398.

Van Den Bos, A., 1971: Alternative interpretation of maximum entropy spectral analysis, *IEEE Trans. Inf. Theory,* **IT-17,** 493–494.

White, W. B., 1977: Annual forcing of baroclinic long waves in the tropical North Pacific. *J. Phys. Oceanogr.,* **7,** 50–61.

——, 1982: Traveling wavelike mesoscale perturbations in the North Pacific Current. *J. Phys. Oceanogr.,* **12,** 231–243.

——, 1985: Resonant response of interannual baroclinic Rossby waves to wind forcing in the eastern midlatitude North Pacific. *J. Phys. Oceanogr.,* **15,** 403–415.

——, and A. E. Walker, 1974: Time and depth scales of anomalous subsurface temperature at Ocean Weather Stations P, N, and V in the North Pacific. *J. Geophys. Res.,* **79,** 4517–4522.

——, and R. L. Bernstein, 1979: Design of an oceanographic network in the midlatitude North Pacific. *J. Phys. Oceanogr.,* **9,** 592–606.

——, and T. F. T. Saur, 1981: A source of annual baroclinic waves in the eastern subtropical North Pacific. *J. Phys. Oceanogr.,* **11,** 1452–1462.

——, and ——, 1983: Sources of interannual baroclinic waves in the eastern subtropical North Pacific. *J. Phys. Oceanogr.,* **13,** 664–673.

——, S. E. Pazan and M. Inoue, 1987: Hindcast/forecast of ENSO events based upon the redistributioin of heat content in the western tropical North Pacific. *J. Phys. Oceanogr.* (in press).

Willmott, A. J., and L. A. Mysak, 1980: Atmospherically forced eddies in the Northeast Pacific. *J. Phys. Oceanogr.,* **10,** 1769–1791.